Ferroelastic Strain Induced Antiferroelectric-Ferroelectric Phase Transformation in Multilayer Thin Film Structures

Meysam Sharifzadeh Mirshekarloo, Kui Yao, and Thirumany Sritharan*

Coupling effects among mechanical, electrical and magnetic parameters in thin film structures including ferroic thin films provide exciting opportunity for creating device functionalities. For thin films deposited on a substrate, their mechanical stress and microstructure are usually determined by the composition and processing of the films and the lattice and thermal mismatch with the substrate. Here it is found that the stress and structure of an antiferroelectric $(Pb_{0.97},La_{0.02})(Zr_{0.90},Sn_{0.05},Ti_{0.05})O_3$ (PLZST) thin film are changed completely by a ferroelastic strain in a magnetic shape memory (MSM) alloy Ni-Mn-Ga (NMG) thin film on the top of the PLZST, despite the existence of the substrate constraint. The ferroelastic strain in the NMG film results in antiferroelectric (AFE) to ferroelectric (FE) phase transformation in the PLZST layer underneath. This finding indicates a different strategy to modulate the structure and function for multilayer thin films and to create unprecedented devices with ferroic thin films.

1. Introduction

Multiferroic thin film materials with the coupling between electric and magnetic order parameters have attracted tremendous interest with the potential in realizing new electromagnetic devices.[1–4] Mechanical stress with pronounced effects on thin film properties provides an extra degree of freedom for tailoring the device functionalities. The stress, typically induced by the thermal and lattice mismatch with the substrate, has widely been investigated and even utilized to tune the crystal symmetry and domain structure of ferroic thin films.[5–14]

In this study, we have found an unusual phenomenon that the transformation from antiferroelectric (AFE) phase to ferroelectric (FE) phase in an antiferroelectric $(Pb_{0.97},La_{0.02})(Zr_{0.90},Sn_{0.05},Ti_{0.05})O_3$ (PLZST) thin film is induced by a ferroelastic strain in a magnetic shape memory (MSM) alloy Ni-Mn-Ga (NMG) thin film deposited on the top of the PLZST thin film, despite the existence of the substrate constraint. The ferroelastic strain in the magnetic NMG top-layer originates from the martensitic phase transformation and the in-plane stress is effectively transmitted to the PLZST sub-layer. As the ferroelastic strains can be modulated by temperature, magnetic field and many other external factors,[15] this finding indicates a new strategy to modulate the structure of ferroic thin films and to create unprecedented device functionalities.

M. S. Mirshekarloo
School of Materials Science and Engineering
Nanyang Technological University
Singapore 639798
Dr. K. Yao
Institute of Materials Research and Engineering
A*STAR (Agency for Science, Technology and Research)
3 Research Link, Singapore 117602
E-mail: k-yao@imre.a-star.edu.sg
Prof. T. Sritharan
School of Materials Science and Engineering
Nanyang Technological University
Singapore 639798

DOI: 10.1002/adfm.201200832

2. Results

160 nm-thick NMG MSM alloy thin film was deposited on a 1.2 μm-thick AFE PLZST thin film on a $Pt/Ti/SiO_2/Si$ substrate. The XRD patterns of the multilayer samples with the as-deposited and annealed NMG thin film (**Figure 1**) were matched with data for NMG and PLZST thin films available in the literature.[16–18] The XRD pattern of the sample with the as-deposited NMG reveals AFE perovskite phase of PLZST with an orthorhombic structure (space group Pbam) in [001] preferential orientation, and an austenite phase (space group $Fm\bar{3}m$) for NMG. After annealing of NMG, the (112), (004) and (200) peaks of the NMG tetragonal martensite phase (space group I4/mmm) appear at 2θ values of 44.3°, 51.4° and 51.8° respectively. Appearance of the minor MnO and $MnGa_2O_4$ phases could be attributed to oxidation at the interface of NMG and PLZST, as observed in cross sectional TEM micrographs (**Figure 2**).

The in-plane and out-of-plane magnetic hysteresis loops indicate that the as-deposited NMG layer is extremely weak magnetic while the annealed NMG is strongly ferromagnetic with an in-plane saturation magnetization of about 190 emu cc^{-1} (**Figure 3**a). This supports the inference from the XRD results that the NMG has transformed from the non-magnetic cubic austenite phase to the magnetic tetragonal martensite phase on annealing.

The phase transformation in the PLZST film from the orthorhombic AFE phase to the rhombohedral FE phase is signified by the appearance of new peaks in the XRD of the annealed sample in Figure 1. This is supported by out-of-plane P-E hysteresis measurements shown in Figure 3b where a well-saturated, single hysteresis loop typical of the FE phase was displayed for the sample after annealing with the martensite NMG layer, while the characteristic double hysteresis loop

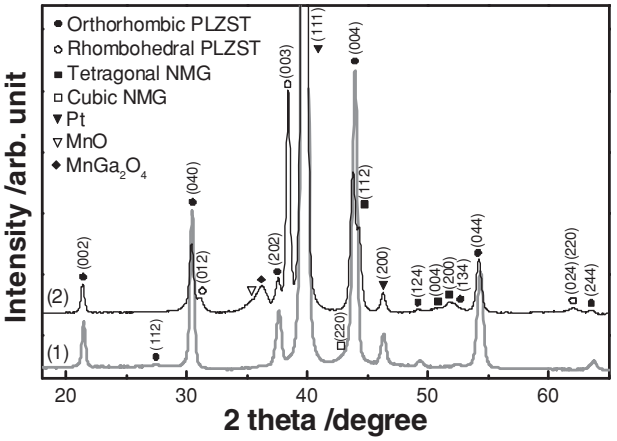

Figure 1. Analysis of crystalline phases in NMG/PLZST multilayer. XRD patterns of NMG/PLZST multilayer on Pt/Ti/SiO_2/Si substrate before (1) and after (2) annealing NMG.

of the AFE phase was obtained for the sample with the as-deposited austenite NMG layer. Thus, AFE to FE phase transformation has occurred in the PLZST film after annealing the NMG top-layer with the martensitic transformation. The small kink detectable at low electric field in the out-of-plane hysteresis loop for the sample with the annealed NMG could be attributed to the minor residual AFE phase as revealed by XRD.

Since inter-diffusion between NMG and PLZST may have triggered such transformation, concentration profiles were determined across the NMG-PLZST interface by secondary ion mass spectroscopy (SIMS) (**Figure 4**). The SIMS study showed some Mn diffusion into PLZST but those of Ni and Ga were negligible. Previous reports in literature on the effects of Mn diffusion into FE Pb(Zr,Ti)O_3, (Pb,La)(Zr,Ti)O_3 and Pb(Zr,Sn,Ti)O_3 show that it promotes the double hysteresis loop in out-of-plane P-E characteristics.[19–21] Consequently, Mn diffusion in PLZST would not have caused the AFE to FE transformation as observed in Figure 3b. Hence, other effects accompanied by the martensitic transformation in the annealed NMG film need be examined.

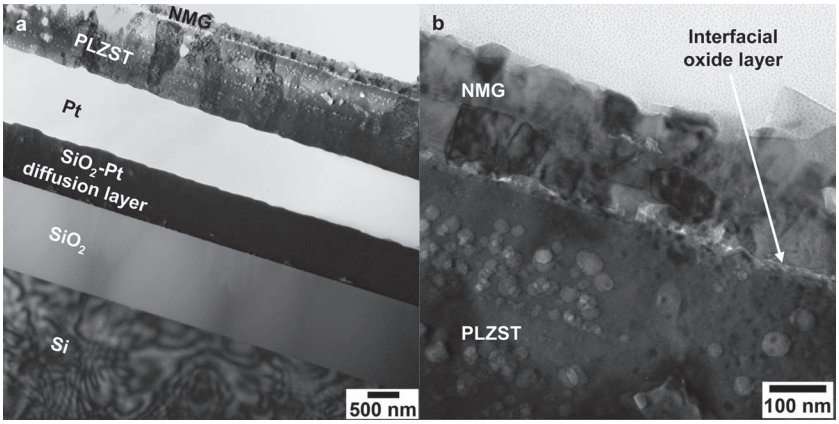

Figure 2. a) Cross sectional bright field TEM micrograph of the NMG/PLZST/Pt/SiO_2/Si multilayer thin film sample. b) An enlarged view of NMG and PLZST interface.

The equivalent residual stress in the PLZST layer was investigated by the $\sin^2\psi$ method.[22] The equivalent residual stress can be derived from a linear fit to the plots of $(d_i\text{-}d_n)/d_n$ against $\sin^2\psi$, as shown in the inset of **Figure 5**a, where d_n and d_i are, respectively, the spacing of the planes parallel to the surface and of the planes whose normal lines have a tilt angle of ψ. The equivalent residual stress determined from this plot for the PLZST film is +60 MPa (tensile) for the sample with the as-deposited austenite NMG and –67 MPa (compressive) with the martensite NMG after annealing. An enlarged view of the (002) and (004) peaks of the orthorhombic PLZST phase in the XRD results is shown in Figure 5a. A peak shift to lower 2θ angles after the NMG martensitic transformation is clear, which represents an increase in the average d-spacing. Since our PLZST film has the preference of [001] orientation, the increase in inter-planar spacing of these planes indicates a compressive in-plane residual stress. This evidence supports our stress measurement results by the $\sin^2\psi$ method. Hence, the AFE to FE transformation observed in the PLZST film accompanied with the NMG martensitic transformation could be attributed to the formation of the in-plane compressive residual stress. In the literature, the appearance of FE phase has been reported in $PbZrO_3$ AFE thin films when a compressive mismatch strain is imposed by the substrate.[23–25]

Another observation, as given in Figure 5b, is that the NMG film thickness increased remarkably from 161 nm to about 199 nm after the annealing and martensitic transformation (measured 10 samples experiencing the same thermal history). Cross-sectional TEM micrographs of the annealed sample revealed an oxide layer at the NMG-PLZST interface, but its thickness was approximately 10 nm (Figure 2b). No surface oxide layer was detectable. Hence, the giant increase in the NMG film thickness cannot be attributed to the oxide formation.

The high resolution transmission electron microscopy (HRTEM) image of the annealed martensite NMG thin film along [$1\bar{1}0$] zone axis revealed a highly deformed and twinned microstructure with large density of dislocations and stacking faults (**Figure 6**a). Because the NMG grain size was small, it was not possible to capture a single crystal diffraction pattern. Hence, fast Fourier transform (FFT) of HRTEM micrograph was used instead. Indexing the FFT of HRTEM micrograph revealed a tetragonal martensite structure for NMG in agreement with the XRD results. The a_M and c_M lattice parameters of the tetragonal structure were determined to be 3.60 and 7.10 Angstroms respectively (inset of Figure 6a).

Since the martensitic transformation in NMG is accompanied by large strain and high strain energy,[26] large stress could be transmitted to the PLZST sub-layer and cause the change from in-plane tensile stress to the compressive stress and thus the compressive strain in the PLZST, through the solidified interface free of delamination as revealed by the cross-sectional TEM examination. The martensitic transformation induced strain could be analyzed from the lattice parameters of the martensite and the austenite phases.

The schematic unit cells of the austenite and martensite phases are displayed in Figure 6b, where it is clear that the tetragonal unit cell

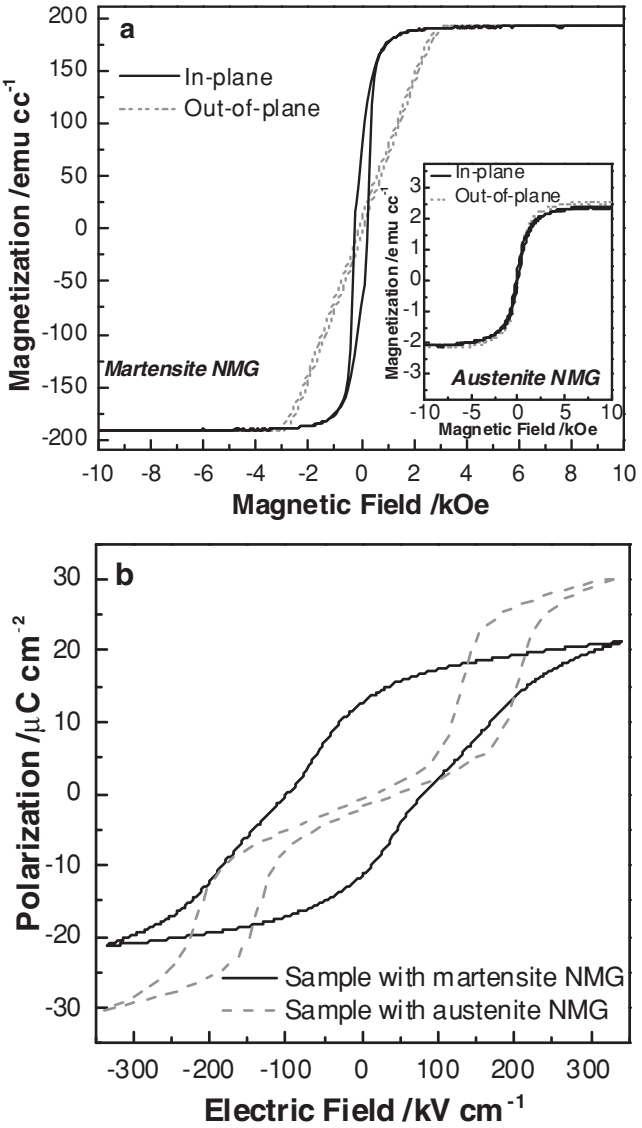

Figure 3. Field dependant magnetization and electrical polarization of NMG/PLZST multilayer. a) Magnetization-magnetic field (*M-H*) hysteresis loops of the austenite and martensite NMG thin films. b) Out-of-plane polarization-electric field (*P-E*) hysteresis loops of the PLZST films with austenite and martensite NMG film on the top, before and after annealing, respectively.

has its fundamental parameters coinciding with the $[1\bar{1}0]_A$, $[110]_A$ and $[001]_A$ directions of the cubic austenite unit cell. Hence, if a martensitic transformation is to be facilitated, a large elongation in the $[001]_A$ direction associated with contractions in $[100]_A$ and $[010]_A$ directions of the parent austenite unit cell are required. The lattice parameters of the deformed parent unit cell can be calculated from the relationships $a'_A = \sqrt{2}a_M$ and $c'_A = c_M$, i. e. $a'_A = 5.09$ Å and $c'_A = 7.10$ Å (Figure 6b). Since the lattice parameter of the austenite parent phase is $a_A = 5.84$ Å, the martensitic transformation will enforce –14.5% strain in $[100]_A$ and $[010]_A$ directions and 21.6% strain in $[001]_A$ direction. If we assume that all 21.6% tensile strain is achieved in out-of-plane direction of NMG, the NMG film could reach a

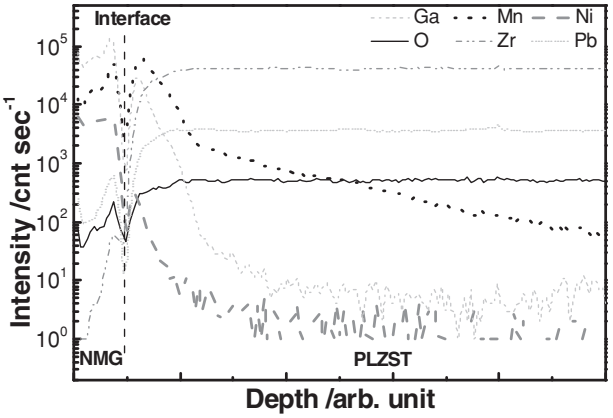

Figure 4. SIMS profile results at the interface of the NMG/PLZST after annealing.

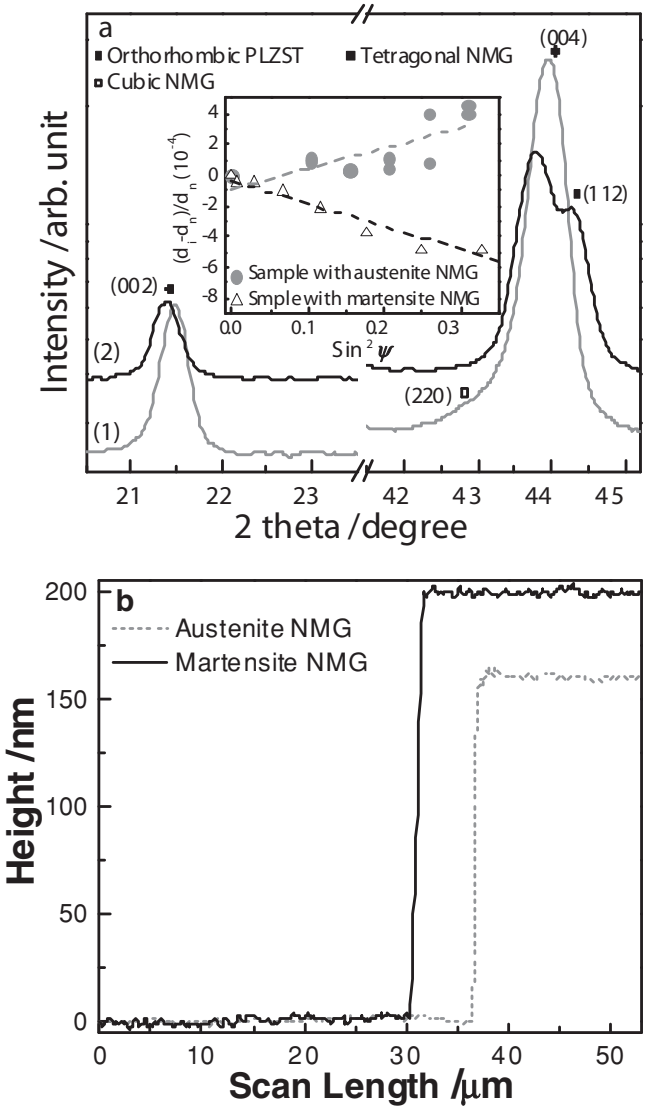

Figure 5. Residual stress and thickness measurements. a) Enlarged view of (002) and (004) peaks of orthorhombic PLZST for the sample with (1) austenite and (2) martensite NMG on the top. The inset presents the plotting and linear fitting of $(d_i–d_n)/d_n$ value against $\sin^2\psi$ for the samples with austenite and martensite NMG. b) Thickness measurement of the austenite and martensite NMG thin films.

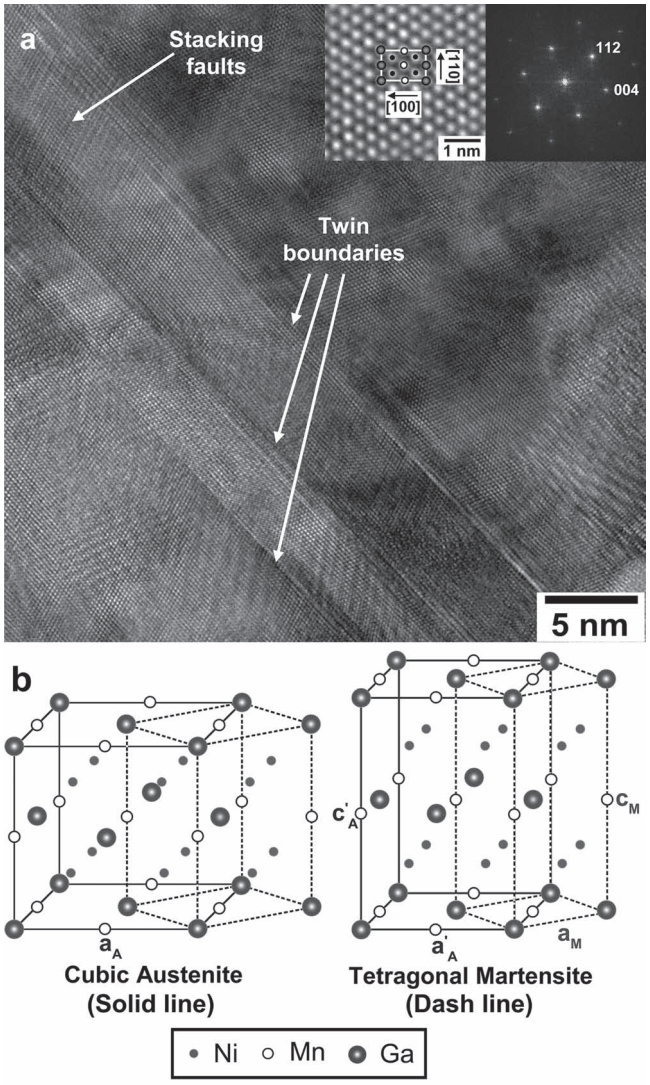

Figure 6. Structural analysis of the martensite NMG thin film. a) HRTEM micrograph of annealed martensite NMG thin film along [1$\bar{1}$0] zone axis. The insets present corresponding FFT micrograph (right) and enlarged view of HRTEM micrograph showing arrangement of Ni, Mn and Ga atoms on (1$\bar{1}$0) plane (left). b) The schematic view of cubic austenite and tetragonal martensite unit cells and the correlation between their lattice parameters.

new thickness of about 195 nm after the transformation. This is in good agreement with our measured thickness of 199 nm for the annealed martensite NMG layer. As a consequence to this large [001] strain, contractions are induced in the in-plane directions of $[100]_A$ and $[010]_A$ of NMG. The Young's modulus of tetragonal martensite NMG (170 GPa)[27] is significantly larger than that of AFE PLZST (60 MPa),[28] which suggests NMG is stiff enough to transfer the in-plane compressive strain to the PLZST sub-layer. However, full strain transfer may not be achievable in practice, because of the constraint from the thick Si substrate. Hence, some relaxation is required in the films, and this is achieved by the formation of twins, stacking faults and dislocations in NMG (as seen in HRTEM micrographs in Figure 6a). As shown in our residual stress measurements for PLZST, some strain is transferred to PLZST, which is adequate to initiate the AFE to FE transformation.

As PLZST is clamped to the substrate, it is likely to have a strain gradient in the case of strain transfer through the interface with the NMG top-layer. To verify this, thin film XRD data was collected at different incident angles (ω), and the position of the (002) peak of the orthorhombic, AFE PLZST film was carefully followed. The incident angle was increased until (111) Pt peak appeared which marks the point of full penetration of the PLZST film by the incident X-rays. The measurements revealed that the peak position shifted to higher angles initially with increasing ω, and finally remained constant beyond ω = 6° (**Figure 7**). This implies that the *c*-lattice parameter of the orthorhombic PLZST phase decreases from the NMG interface towards the substrate interface, indicating a decreasing compressive residual strain across the film thickness. Thus, near the substrate interface, the strain may be too low to initiate the AFE to FE transformation. This could explain the existence of the residual AFE phases within the PLZST film after the NMG annealing, as shown by the XRD and the out-of-plane polarization hysteresis loop measurements.

Typical energy barrier for phase transformation between various AFE and FE or paraelectric phases in $PbZrO_3$-based AFE systems is estimated to be of the order of 10 J cm^{-3}.[29,30] The maximum strain energy per unit volume induced in PLZST by the martensitic transformation in NMG can be estimated as $\frac{1}{2}\sigma.\epsilon = \frac{1}{2}\frac{\sigma^2}{E}$, where σ, ε and E are stress, strain and Young's modulus of PLZST. This is about 134.5 J cm^{-3}, which is significantly larger than the barrier energy for the phase transformation, and hence even a fraction of it is adequate to induce the transformation from orthorhombic AFE phase to rhombohedral FE phase.

To study the reversible transformation between the FE and AFE phases in PLZST, high temperature XRD studies were conducted. However, we found that the martensite to austenite

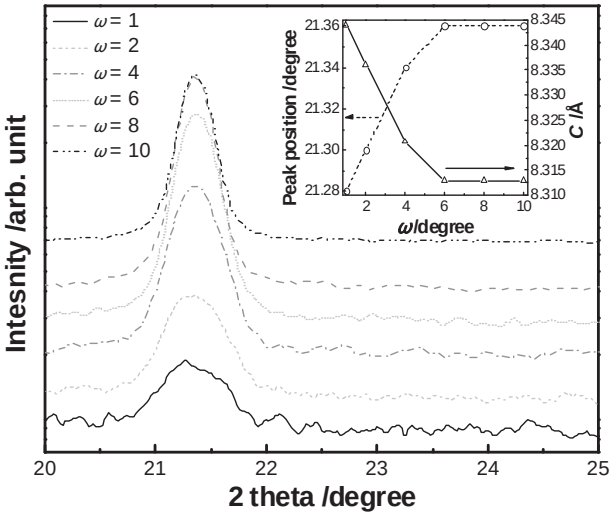

Figure 7. XRD measurements of (002) peak of the orthorhombic PLZST phase in the annealed multilayer sample at different X-ray incident angles (ω). The inset shows the (002) peak position and the c-lattice parameter of the orthorhombic PLZST phase as a function of the incident angle.

transformation temperature of NMG thin film with current composition (about 350 °C) was higher than the Curie temperature of PLZST (about 270 °C). It is possible to change the composition of NMG for reducing the martensite to austenite transformation temperature to below the Curie temperature of an antiferroelectric material for studying the reverse transformation. Appropriate change of the compositions of the antiferroelectric films could also facilitate reverse FE to AFE transformation.

As ferroelastic strain accompanying the martensitic phase transformation in many ferromagnetic thin films can be modulated by temperature, magnetic field and many other external factors, this finding suggests that the ferroelectric order parameters can be potentially controlled through many other thermal, magnetic, and mechanical parameters. The strong mechanical coupling and the correspondingly induced phase transitions between the multilayer thin films beyond the restriction of the substrate indicates a generally new strategy to modulate the structure and properties of ferroic thin films. For example, it is well known that magnetic shape memory alloy single crystals can induce large strain under applied magnetic field (up to 10%), which in principal can be used to force the transformation between different phases of PLZST. For magnetic shape memory alloy thin films, it is still a challenge to induce such large magnetic field induced strain due to the effects of stress, imperfections and small grains. The finds here will inspire many different methodologies and designs to be proposed for creating unprecedented device functionalities.

3. Conclusions

With detailed structural analyses on a magnetic shape memory (MSM) alloy Ni-Mn-Ga (NMG) thin film deposited on an antiferroelectric $(Pb_{0.97},La_{0.02})(Zr_{0.90},Sn_{0.05},Ti_{0.05})O_3$ (PLZST) film, it is revealed that a large ferroelastic strain was generated in the NMG film originated from the martensitic phase transformation. The ferroelastic strain was coupled to the PLZST sub-layer and caused the stress change from in-plane tensile stress to the compressive stress in the PLZST, despite the existence of the substrate constraint, which further resulted in antiferroelectric (AFE) to ferroelectric (FE) phase transformation in the PLZST layer. This finding indicates a different strategy to modulate the structure and function for multilayer thin films, and to create unprecedented devices with ferroic thin films.

4. Experimental Section

The chemical solution deposition process, structure and electrical properties of the AFE PLZST thin films on $Pt/Ti/SiO_2/Si$ substrate were reported in our previous publication.[31]

The NMG thin films were grown on 1.2 μm-thick PLZST sub-layer at room temperature in a Denton DC sputtering system using a target with a nominal alloy composition of $Ni_{49.5}Mn_{28.0}Ga_{22.5}$. The sputtering deposition was performed in a vacuum of 5×10^{-7} Torr, at a deposition power of 30 W DC and argon pressure of 3×10^{-3} Torr. A pre-sputtering treatment was done for 30 minutes to achieve stable plasma and to remove oxides from the surface of the target. The deposition time was adjusted to achieve a thickness of 160 nm. The deposited NMG thin films on the top of the PLZST layer were annealed at 650 °C for 10 min in nitrogen atmosphere using a rapid thermal annealing (RTA) system at a heating rate of 20 °C sec^{-1}. After annealing, the films were cooled to room temperature over 15 min.

The crystalline phases and equivalent residual stress of the thin films were examined using Bruker D8-Advance and PANalytical X'Pert PRO diffractometers (Cu-K radiation) and JEOL JSM-2100F transmission electron microscope (TEM). Cross-sectional TEM samples were prepared by conventional mechanical grinding and Ar^+ ion milling to achieve electron transparency. The temperature of the sample was kept at room temperature during the process by a cooling system to avoid any temperature-induced transformation. Element concentration depth profiling was carried out using secondary ion mass spectroscopy (SIMS) (ION-ToF GmbH, Heisenbergstr, Munster, Germany) to study the inter-diffusion between PLZST and NMG layers.

In-plane and out-of-plane magnetic field dependant magnetization loops were measured using a MicroMag 2900 alternating gradient magnetometer (AGM). Out-of-plane Polarization-electric field (*P-E*) characteristics were evaluated with a standard RT66A (Radiant Technologies) testing unit.

Acknowledgements

The authors would like to acknowledge the research grant support (IMRE/10-1C0109) and facility support at SNFC from Institute of Materials Research and Engineering, A-STAR (Agency for Science, Technology and Research), Singapore.

Received: March 24, 2012
Revised: April 16, 2012
Published online: June 8, 2012

[1] R. Ramesh, N. A. Spaldin, *Nat. Mater.* **2007**, *6*, 21.
[2] M. Bibes, A. Barthelemy, *Nat. Mater.* **2008**, *7*, 425.
[3] N. A. Spaldin, M. Fiebig, *Science* **2005**, *309*, 391.
[4] I. Stolichnov, S. W. E. Riester, H. J. Trodahl, N. Setter, A. W. Rushforth, K. W. Edmonds, R. P. Campion, C. T. Foxon, B. L. Gallagher, T. Jungwirth, *Nat. Mater.* **2008**, *7*, 464.
[5] C. Ederer, N. A. Spaldin, *Phys. Rev. Lett.* **2005**, *95*, 257601.
[6] G. Catalan, A. Janssens, G. Rispens, S. Csiszar, O. Seeck, G. Rijnders, D. H. A. Blank, B. Noheda, *Phys. Rev. Lett.* **2006**, *96*, 127602.
[7] M. Marsilius, J. Frederick, W. Hu, X. Tan, T. Granzow, P. Han, *Adv. Funct. Mater.* **2012**, *22*, 797.
[8] Z. Chen, Z. Luo, C. Huang, Y. Qi, P. Yang, L. You, C. Hu, T. Wu, J. Wang, C. Gao, T. Sritharan, L. Chen, *Adv. Funct. Mater.* **2011**, *21*, 133.
[9] J. Wang, J. B. Neaton, H. Zheng, V. Nagarajan, S. B. Ogale, B. Liu, D. Viehland, V. Vaithyanathan, D. G. Schlom, U. V. Waghmare, N. A. Spaldin, K. M. Rabe, M. Wuttig, R. Ramesh, *Science* **2003**, *299*, 1719.
[10] W. Eerenstein, F. D. Morrison, J. Dho, M. G. Blamire, J. F. Scott, N. D. Mathur, *Science* **2005**, *307*, 1203a.
[11] J. Wang, A. Scholl, H. Zheng, S. B. Ogale, D. Viehland, D. G. Schlom, N. A. Spaldin, K. M. Rabe, M. Wuttig, L. Mohaddes, J. Neaton, U. Waghmare, T. Zhao, R. Ramesh, *Science* **2005**, *307*, 1203b.
[12] K. J. Choi, M. Biegalski, Y. L. Li, A. Sharan, J. Schubert, R. Uecker, P. Reiche, Y. B. Chen, X. Q. Pan, V. Gopalan, L.-Q. Chen, D. G. Schlom, C. B. Eom, *Science* **2004**, *306*, 1005.
[13] R. J. Zeches, M. D. Rossell, J. X. Zhang, A. J. Hatt, Q. He, C.-H. Yang, A. Kumar, C. H. Wang, A. Melville, C. Adamo, G. Sheng, Y.-H. Chu, J. F. Ihlefeld, R. Erni, C. Ederer, V. Gopalan, L. Q. Chen, D. G. Schlom, N. A. Spaldin, L. W. Martin, R. Ramesh, *Science* **2009**, *326*, 977.

[14] J. X. Zhang, B. Xiang, Q. He, J. Seidel, R. J. Zeches, P. Yu, S. Y. Yang, C. H. Wang, Y.-H. Chu, L. W. Martin, A. M. Minor, R. Ramesh, *Nat. Nanotechnol* **2011**, *6*, 98.
[15] K. Ullakko, J. K. Huang, C. Kantner, R. C. O'Handley, V. V. Kokorin, *Appl. Phys. Lett.* **1996**, *69*, 1966.
[16] S. Teslic, T. Egami, *Acta Crystallogr. Sec. B* **1998**, *54*, 750.
[17] D. Y. Cong, P. Zetterström, Y. D. Wang, R. Delaplane, R. L. Peng, X. Zhao, L. Zuo, *Appl. Phys. Lett.* **2005**, *87*, 111906.
[18] D. Y. Cong, Y. D. Wang, P. Zetterström, R. L. Peng, R. Delaplane,, X. Zhao, L. Zuo, *Mater. Sci. Technol.* **2005**, *21*, 1412.
[19] Z. Cao, A. Ding, Y. Zhang, P. Qiu, X. Zheng, *Solid State Commun.* **2004**, *131*, 57.
[20] A. Pathak, R. Chatterjee, C. Prakash, *Ceram. Int.* **2010**, *36*, 2263.
[21] Y. Pu, J. Zhu, X. Zhu, Y. Luo, M. Wang, X. Li, J. Liu, J. Zhu, D. Xiao, *J. Appl. Phys.* **2011**, *109*, 044102.
[22] K. Yao, S. Yu, F. E. H. Tay, *Appl. Phys. Lett.* **2003**, *82*, 4540.
[23] K. Boldyreva, L. Pintilie, A. Lotnyk, I. B. Misirlioglu, M. Alexe, D. Hesse, *Appl. Phys. Lett.* **2007**, *91*, 122915.
[24] K. Boldyreva, L. Pintilie, A. Lotnyk, I. B. Misirlioglu, M. Alexe, D. Hesse, *Ferroelectrics* **2008**, *370*, 140.
[25] A. R. Chaudhuri, M. Arredondo, A. Hähnel, A. Morelli, M. Becker, M. Alexe, I. Vrejoiu, *Phys. Rev. B* **2011**, *84*, 054112.
[26] R. C. O'Handley, *J. Appl. Phys.* **1998**, *83*, 3263.
[27] S. Ozdemir Kart, T. Cagin, *J. Alloys Compd.* **2010**, *508*, 177.
[28] Q. M. Zhang, Z. Zhao, *IEEE Trans. Ultrason. Ferroelectr. Freq. Control.* **1999**, *46*, 1518.
[29] D. Berlincourt, H. H. A. Krueger, B. Jaffe, *J. Phys. Chem. Solids.* **1964**, *25*, 659.
[30] P. Yang, D. A. Payne, *J. Appl. Phys.* **1992**, *71*, 1361.
[31] M. Sharifzadeh Mirshekarloo, K. Yao, T. Sritharan, *Appl. Phys. Lett.* **2010**, *97*, 142902.